Ultrafast white-light continuum generation and self-focusing in transparent condensed media

A. Brodeur* and S. L. Chin

Centre d'Optique, Photonique et Laser and Département de Physique, Université Laval, Québec G1K 7P4, Canada

We report an investigation of white-light continuum generation and self-focusing by 140-fs Ti:sapphire laser pulses in extended transparent media. It is found that continuum generation is triggered by self-focusing and that both phenomena depend on the medium's bandgap. There is a bandgap threshold for continuum generation. Above that threshold the continuum's width increases with increasing bandgap. Furthermore, the beam's self-focal diameter is discontinuous across the threshold. To explain the observations a mechanism is proposed that involves multiphoton excitation of electrons into the conduction band at the self-focus; the generated free electrons cause spectral superbroadening and limit the self-focal diameter. The continuum beam's surprisingly low divergence is then investigated and explained in terms of a Kerr lensing effect. © 1999 Optical Society of America [S0740-3224(99)00204-0]

OCIS codes: 320.7110, 320.7120, 320.2250, 190.5940, 190.4180, 190.2620.

1. INTRODUCTION

The propagation of powerful ultrashort laser pulses in transparent media can give rise to one of the most spectacular phenomena of nonlinear optics: superbroadening of the pulse's spectrum into a white-light continuum, also called a supercontinuum.[1–15] This well-known phenomenon can occur in a wide variety of transparent condensed media[1–6,8,11,13,15] and in gases.[2,7,9,10]

The ultrafast white-light continuum is useful for various applications as a tunable ultrafast light source. Among these we find time-resolved broadband absorption and excitation spectroscopy,[2] optical parametric amplification,[16] and dynamic characterization of laser-induced structural transitions.[17] The continuum can also be used for optical pulse compression.[2]

The first observation of the white-light continuum dates back to the late 1960's, when Alfano and Shapiro focused powerful picosecond pulses into glass samples.[1] The continuum that they observed covered the visible spectral range and extended into the near infrared. In 1983 Fork *et al.* generated the first femtosecond continuum by focusing powerful 80-fs pulses into an ethylene glycol film[6]; the resultant continuum ranged from the ultraviolet to the near infrared. Continuum generation in gases by femtosecond pulses was then demonstrated by Corkum *et al.*[7]

The general characteristics of the femtosecond continuum are as follows: Its spectral width depends on the medium in which it is generated,[18] its spectrum is modulated,[1] its polarization is in the same direction as the polarization of the input pulse,[18] and its anti-Stokes frequency components lag temporally its Stokes components.[6,19] The femtosecond continuum exhibits a smaller beam divergence than the picosecond continuum.[7] When it is projected onto a screen the femtosecond continuum beam appears to the eye as a white disk, often surrounded by a distinct concentric rainbow-like pattern (conical emission). For clarity, the term "white-light continuum" will hereafter refer to the low-divergence, central part of the beam and exclude the conical emission.

Despite its widespread use the white-light continuum remains far from being well understood. Especially intriguing is the mechanism that determines its spectral width. Among the various mechanisms that have been suggested so far, we find self-phase modulation (SPM),[1,6,8] ionization-enhanced SPM,[4,5] and four-wave mixing.[1,3,12,14] It is at present generally believed that the main mechanism in femtosecond continuum generation is SPM enhanced by self-steepening of the pulse.[2,8] A shortcoming of this model is its prediction of a broader continuum in media with higher Kerr nonlinearity, a trend that is not observed.[2,11] For instance, the continuum generated in water is among the broadest observed, despite the particularly low Kerr nonlinearity of water.

Self-focusing is believed to play an important role in continuum generation in extended media. Experiments have shown that the power threshold for continuum generation coincides with the calculated critical power for self-focusing.[5,7,10,15] This is not surprising, considering that the onset of catastrophic self-focusing at critical power leads to a drastic increase in intensity,[20,21] which can enhance SPM. However, this coincidence also suggests an intimate connection between the continuum and the mechanism that stops catastrophic self-focusing. Such a connection was first proposed by Bloembergen[4] to explain the picosecond continuum. In his model self-focusing is stopped by avalanche ionization; the appearance of free electrons enhances SPM and results in the continuum. A similar mechanism can be envisaged for femtosecond continuum generation in condensed media.

In this case an important mechanism of free-electron generation is multiphoton excitation (MPE).[22,23]

To better understand continuum generation and self-focusing in the femtosecond regime it would be useful to monitor experimentally the evolution of the pulsed laser beam as it undergoes these processes. This approach was used in 1966 by Garmire *et al.* in a study of self-focusing of nanosecond pulses in CS_2.[24] In that experiment the evolution of the beam profile was measured by insertion of beam splitters at various positions along the CS_2 cell. A different approach was used by Loy and Shen[25]; in their experiment they measured the beam profile by imaging the beam at a point in the medium, using a lens located in the beam path at the output of the medium. In the present study these concepts are used in a new technique of imaging spectroscopy in which the beam profile, the pulse spectrum, and the pulse energy can be measured at any point along the propagation axis.[26]

In this paper we investigate the mechanisms that govern superbroadening and self-focusing of 140-fs Ti:sapphire laser pulses in condensed media. The results confirm that continuum generation is triggered by self-focusing and reveal a strong dependence of continuum generation and self-focusing on the medium's bandgap. A bandgap threshold is found below which the medium cannot generate a continuum and above which the continuum width increases with the bandgap. This observation contradicts the theory of SPM in a neutral Kerr medium, the mechanism that is generally accepted as being responsible for continuum generation. Enhancement of SPM by free electrons generated by MPE is proposed as the primary mechanism of continuum generation. The continuum beam's anomalous divergence[7] is also investigated. It is found that the small divergence of the continuum beam does not imply the absence of strong self-focusing but is rather due to a self-guiding mechanism that involves the Kerr effect. Some of the results presented in this paper were reported in a previous Letter.[27]

Section 2 is a survey of the main mechanisms known to be involved in the propagation of powerful laser pulses. The experimental setup is presented in Section 3, followed in Section 4 by an experimental description of continuum generation and self-focusing. The mechanism that limits self-focusing and the mechanism that is responsible for continuum generation are investigated in Subsections 5.A and 5.B, respectively. The continuum beam's anomalous divergence is investigated in Section 6. Finally, the results are summarized in Section 7.

2. SURVEY

The Kerr nonlinearity, or intensity-dependent refractive index, is a dominant nonresonant nonlinearity. In the femtosecond regime it is due mainly to a distortion of the electron cloud and has a time response of the order of an electronic orbital period ($\sim 10^{-16}$ s),[28] which is much shorter than the pulse duration. Two important effects associated with this nonlinearity are self-focusing and SPM. Because all transparent media possess an electronic Kerr nonlinearity these effects can occur in any transparent medium; they are therefore important in any application involving the propagation of powerful ul-

trashort pulses. In typical condensed media peak powers in the megawatt range are required for self-focusing and self-phase modulation to be important.

A. Self-Focusing
Self-focusing[20,21] is a well-known phenomenon that arises in the propagation of a powerful laser beam in a Kerr medium, in which the index of refraction is $n = n_0 + n_2 I$ (n_0 is the linear index of refraction, n_2 is the nonlinear index of refraction, and I is the field intensity). For a cw Gaussian beam, catastrophic self-focusing occurs at powers that exceed the critical power[20]

$$P_{\text{crit}} = \frac{3.77 \lambda_0{}^2}{8 \pi n_0 n_2},\tag{1}$$

where λ_0 is the laser wavelength. The Gaussian beam then collapses to a singularity at a distance[20]

$$z_f(P) = \frac{0.367 k a_0{}^2}{[(\sqrt{P/P_{\text{crit}}} - 0.852)^2 - 0.0219]^{1/2}},\tag{2}$$

where P is the beam power, $k = 2\pi/\lambda_0$ is the wave number, and a_0 is the input beam's radius at the $1/e$ level of intensity. This distance is measured from the waist of the Gaussian beam at the medium's entrance.

In most experimental investigations of self-focusing an external lens is used to force self-focusing within the length of the medium. For a lens with focal length f we obtain the self-focusing distance z_f' by using the lens transformation[29]

$$z_f' = \frac{z_f f}{z_f + f}.\tag{3}$$

With positive focusing we thus have $z_f' \leq f$, i.e., the self-focus occurs before the geometrical focus.

For a laser pulse the beam power P varies with time. In the slowly varying envelope approximation (which is valid for pulses as short as roughly 10 optical cycles,[30] or ~ 30 fs at 800 nm) and in the approximation of a dispersionless medium, self-focusing can be described in terms of the moving-focus model.[20,21] The laser pulse is then viewed as consisting of a longitudinal stack of infinitely thin transverse slices that propagate independently from one another at the pulse's group velocity. Each slice behaves according to its own power; the slices with power exceeding P_{crit} undergo a collapse at a distance given by Eq. (2). Because the position of the self-focus depends on power, various slices will collapse at different positions. When the pulse is much shorter than the self-focusing distance the first slice to self-focus is the most powerful slice at the center of the pulse. This implies that an intensity spike develops initially at the center of the pulse during self-focusing.

Medium dispersion can be important when one is considering self-focusing of ultrashort pulses. The connection among self-focusing, group-velocity dispersion (GVD), and SPM has been investigated.[15,31–36] During self-focusing an ultrashort pulse broadens spectrally because of SPM, but the new frequency components suffer a temporal rearrangement that is due to GVD. This causes a reduction of peak power during self-focusing, such that a higher input power is required for the onset of

catastrophic self-focusing. Therefore P_{crit} is higher for ultrashort pulses than for long pulses.[31,32,34] The temporal rearrangement of the frequency components as a result of GVD during self-focusing can also result in a temporal splitting of the pulse.[33] An experimental observation of pulse splitting was reported in Refs. 15, 35, and 36.

B. Limitation of Self-Focusing

The transverse diameter of a self-focus is expected to be limited to a finite size by mechanisms that compete with the Kerr nonlinearity. Nonparaxial calculations have shown that diffraction should stop the collapse at a self-focal diameter of approximately one optical wavelength.[37] However, high intensities are achieved before this lower limit is attained, and the approximation of a strictly Kerr nonlinearity does not hold.

The generation of free electrons is an important mechanism that limits self-focusing in condensed media.[38] Free electrons induce a negative change in the index of refraction, which is given in the Drude approximation by (in electrostatic units)[39]

$$\Delta n_e = -\frac{2\pi e^2 N_e}{n_0 m_e(\omega_0^2 + \nu^2)}, \tag{4}$$

where N_e is the electron density, ν is the electron collision frequency, and ω_0 is the laser frequency. When N_e reaches $\sim 10^{17}$–$10^{18}\,\mathrm{cm}^{-3}$ the Kerr index $n_2 I$ is canceled by Δn_e, and self-focusing stops.[38]

Two important mechanisms of free-electron generation by a laser field in condensed matter are MPE and avalanche ionization. The Keldysh theory of MPE in condensed matter[40] calculates perturbatively the transition rate W of an electron from an initial state in the valence band of the material to a final state in the conduction band, where it is essentially free[41] and oscillates in the laser field. In that transition the electron gains an energy in excess of the bandgap energy E_{gap} between the valence and conduction bands. In the regime considered in this study, the dependence of W on intensity I is of the type $W \propto I^N$, where N is the integer part of $[(E_{\mathrm{gap}}/\hbar\omega_0) + 1]$ and ω_0 is the laser frequency.

In avalanche ionization a seed electron (generated by ionization of a shallow trap or an impurity) is heated by the laser field until it has sufficient energy to excite another electron into the conduction band by collision. These two electrons then go on and excite two more electrons, and so on. In this avalanche process the free-electron density N_e grows exponentially.[38] Avalanche ionization requires lower intensities than multiphoton ionization but it also requires time to build up. The relative importance of MPE and avalanche ionization depends on the pulse duration.

In the nanosecond pulse regime stimulated Raman scattering can contribute to the limitation of self-focusing by depleting the pulse energy.[42] On the other hand, with femtosecond pulses self-focusing can ultimately be stopped by GVD by temporal stretching of the pulse.[32,34]

C. Self-Phase Modulation

SPM[20,21,43] arises from the temporal distribution of nonlinear phase in a laser pulse, in much the same way that self-focusing arises from the spatial distribution of nonlinear phase in a laser beam. A laser pulse with on-axis intensity distribution $I(z, \tau)$ that propagates over a distance L in a medium with index $n = n_0 + n_2 I$ will accumulate an on-axis nonlinear phase distribution

$$\phi_{\mathrm{NL}}(\tau) = \int_0^L n_2 I(z, \tau) \frac{\omega_0}{c} \mathrm{d}z, \tag{5}$$

where c is the speed of light. The spectrum implied by this nonlinear phase covers frequencies ranging from the maximum Stokes extent

$$\Delta\omega_-{}^{\mathrm{SPM}} = \left(-\frac{\mathrm{d}\phi_{\mathrm{NL}}}{\mathrm{d}\tau}\right)_{\min} \tag{6}$$

to the maximum anti-Stokes extent

$$\Delta\omega_+{}^{\mathrm{SPM}} = \left(-\frac{\mathrm{d}\phi_{\mathrm{NL}}}{\mathrm{d}\tau}\right)_{\max}. \tag{7}$$

One sees that $\Delta\omega_-{}^{\mathrm{SPM}}$ ($\Delta\omega_+{}^{\mathrm{SPM}}$) is given by the maximum rate of increase (decrease) of the nonlinear phase along the pulse.

In simple SPM theory[30,44] the pulse intensity $I(\tau)$ does not vary with propagation distance z. The accumulated nonlinear phase is thus proportional to the pulse's intensity envelope. The instantaneous frequency is then Stokes shifted (i.e., redshifted) at the front of the pulse and anti-Stokes shifted (i.e., blue shifted) at the back of the pulse.

SPM in the ultrafast regime should be quite strong because the Stokes (anti-Stokes) broadening is inversely proportional to the pulse's rise time (decay time). The rigorous theory of strong SPM developed in Ref. 8 yields an asymmetrical broadening that is stronger on the anti-Stokes side than on the Stokes side. For the hyperbolic secant input pulse $E_0(r, \tau) = E_0(r)\mathrm{sech}(\tau/\tau_0')$, the broadening is given by

$$\frac{\Delta\omega_\pm{}^{\mathrm{SPM}}}{\omega_0} = 1/2(\sqrt{Q^2 + 4} \pm |Q|) - 1, \tag{8}$$

where $Q = 2n_2 I L/c\tau_0'$. For $Q \ll 1$, Eq. (8) reduces to simple SPM theory. This asymmetrical broadening is obtained in the approximation of a constant pulse shape. The asymmetry is more pronounced when self-steepening is taken into account.[8]

The SPM theory discussed so far arises from the Kerr nonlinearity. However, free-electron generation by the laser pulse can also contribute to SPM. The nonlinear index change is then a combination of the Kerr index $n_2 I$ and the free-electron index Δn_e; the latter, being negative, contributes to enhance anti-Stokes SPM. This mechanism is discussed further in Subsection 5.B.

3. EXPERIMENTAL SETUP

With the setup of Fig. 1 the beam profile, the pulse spectrum, and the pulse energy can be measured at any point
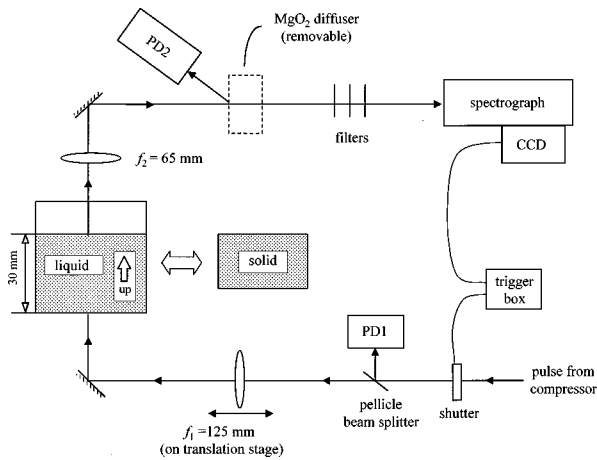
Fig. 1. Experimental setup for measuring the evolution of the beam profile, the pulse spectrum, and the pulse energy during propagation.

along the propagation axis during self-focusing and white-light continuum generation in condensed media.[26]

The input laser pulses are produced by a Ti:sapphire chirped-pulse amplification laser chain (Clark-MXR CPA-1). The chain generates a 1-kHz pulse train, from which a 10-Hz beam is sliced and sent to the setup. The pulse duration is 140 fs FWHM (transform limited), and the central wavelength is $\lambda_0 = 796$ nm. The pulse energy is attenuated before the compressor with a half-wave plate followed by a polarizer. The resultant pulse energy is typically of the order of 1 μJ. The beam is spatially filtered before the compressor, and the central part of the resulting Airy pattern is selected with an iris, producing a beam with radius $a_0 = 0.80$ mm (1/e of fluence). One obtains the latter beam by sending the first beam through an iris and measuring the iris diameter for which 63% of the pulse energy is transmitted.

The beam enters the setup of Fig. 1 through a mechanical shutter activated by a trigger box synchronized with the laser chain. The shutter selects a single pulse from the 10-Hz train. The energy of the input pulse is measured with calibrated photodiode PD1, which detects the partial reflection from a pellicle beam splitter. Only the laser shots with energy within ±1% of the desired input energy are recorded. After the beam splitter the beam is focused with lens f_1 (focal length, 125 mm) into the solid or liquid, where it propagates vertically upward. The liquids are contained in a cylindrical stainless-steel cell equipped with fused-silica windows at both ends. The diameter of the cell is 75 mm, its length is 70 mm, and the depth of the liquid within the cell (i.e., the thickness of liquid through which the pulse propagates) is 30 mm. The cell window is 3 mm thick, and its diameter is 25 mm. We study the propagation in solids by replacing the cell with various solid samples with the following thicknesses: LiF, 10 mm; CaF_2, 6.2 mm, UV-grade fused silica, 10 mm; NaCl, 20 mm; SF-11 glass, 10 mm.

We measure the pulse's spectrum and beam profile by imaging the output surface of the medium with lens f_2 (focal length, 65 mm; achromatic, UV cutoff at 350 nm or 28 500 cm^{-1}) onto the entrance slit of the spectrograph. The distance between lens f_2 and the slit (image plane) is

96 cm, for a magnification of 29.2. The imaging resolution is ~5 μm. Images are captured on a single-shot basis with a cryogenically cooled charge-coupled device (CCD) detector. The CCD is located at the image plane of the spectrograph and is activated by the trigger box. We measure the beam profile by opening the slit of the spectrograph and setting the spectrograph to zero order and measure the spectrum by closing the slit to 50 μm and setting the spectrograph to first order. Filters are used to isolate different parts of the spectrum: BG18 for $\lambda < 630$ nm and RG850 for $\lambda > 850$ nm. All spectra shown are corrected for filter, grating, and CCD responses. The total transmitted pulse energy (hence energy loss) is measured with calibrated photodiode PD2 detecting light scattered by a (removable) MgO_2 diffuser and averaged over 50 shots. The photodiode signal is corrected for the photodiode's spectral response when the measured pulse has a broad spectrum (for a continuum pulse this correction is typically ~1%).

We choose to image the medium's output surface rather than a plane in the bulk of the medium to avoid nonlinear propagation between the object and image planes of lens f_2, which would introduce aberrations. The propagation from the medium's output surface to the slit of the spectrograph occurs in air, which can be considered a linear medium in this experiment. When it is going through lens f_2 the beam has a large diameter, and the propagation is essentially linear.

To measure the pulse at different stages of propagation in the medium we move focusing lens f_1 upon a translation stage. For instance, to measure the geometrical focus of the beam we position lens f_1 such that the geometrical focus is at the output surface of the medium. A displacement of f_1 by an amount Δz away from the medium implies an increase by Δz of the optical path s from the lens to the medium's output surface. Displacing the lens by Δz is thus equivalent to increasing the length of the medium by $\Delta z/n_0$ (and still measuring the beam at the output surface). Therefore, moving lens f_1 away from the medium by Δz yields a measurement of the beam at a stage of propagation farther by $\Delta z/n_0$ along the propagation axis.

4. MEASUREMENT OF CONTINUUM GENERATION AND SELF-FOCUSING

In this section we describe various aspects of self-focusing and continuum generation in condensed media, as measured with the setup of Fig. 1.

A. Effect of Self-Focusing on the Beam Focus
In the linear regime (i.e., at low power) the diameter of the beam focus in the medium is determined by the diameter of the input beam and the focal length of the focusing lens. The situation is expected to be different at high power, when self-focusing imposes additional beam contraction. When the beam power equals the critical power P_{crit} we expect a self-focus to form at the geometrical focus (see Subsection 2.A). At higher power, the self-focus should form at a position closer to the medium entrance. Let us see how self-focusing affects the beam profile at the geometrical focus in water.

We measure the beam profile at the geometrical focus (i.e., at the beam waist) by positioning lens f_1 such that the geometrical focus is at the output surface of the medium. We do this by moving lens f_1 until the diameter of the beam's image on the CCD detector is minimized. There is $\pm{\sim}200\ \mu$m uncertainty in the position of f_1 with this procedure because of the depth of the beam's focus. We then observe the effect of self-focusing by varying the pulse's input peak power.

At low power the FWHM beam waist is $d \simeq 27\ \mu$m. This linear-regime diameter is determined by the focusing geometry and the refractive index of water. d decreases with increasing power, reaches a minimum $d_{\min}$, and then increases [Fig. 2(a)]. Note that d is the time-integrated diameter and is larger than the actual self-focal diameter, as we discuss further in Subsection 5.A below. We define the threshold power for self-focusing $P_{\text{th}}^{\text{sf}}$ as the input peak power at the entrance of the medium for which $d_{\min}$ occurs. Figure 2(b) shows the beam profile that corresponds to $d_{\min}$ in water. In the approximation of a strictly Kerr nonlinearity and a dispersionless and absorptionless medium, $P_{\text{th}}^{\text{sf}}$ would be equal to P_{crit} because the self-focus would occur at the geometrical focus of the focusing lens [Eqs. (2) and (3)].

When the power is increased above $P_{\text{th}}^{\text{sf}}$ the position where $d_{\min}$ occurs moves toward the entrance of the medium. For all investigated media $d_{\min}$ occurs at ${\sim}500$ μm before the geometrical focus when $P = 1.1P_{\text{th}}^{\text{sf}}$, in agreement with Eqs. (2) and (3). Diameter $d_{\min}$ remains practically constant at powers above $P_{\text{th}}^{\text{sf}}$. For instance, in water $d_{\min}$ remains within 0.5 μm of 10 μm from $P = 1.1P_{\text{th}}^{\text{sf}}$ to $P = 2P_{\text{th}}^{\text{sf}}$. The so-called filament associated with these dynamics is discussed in Subsection 4.B.

The reduction of focal diameter that results from an increase of power toward $P_{\text{th}}^{\text{sf}}$ causes a drastic increase in focal intensity. In water, for instance, the focal spot rapidly shrinks from the linear focal diameter $d \simeq 27\ \mu$m to a self-focal diameter of less than 10 μm. This implies a more than tenfold increase in intensity. We shall see in Subsection 4.B that this increase triggers continuum generation.

B. Continuum Generation during Self-Focusing

In most media a threshold peak power $P_{\text{th}}^{\text{wl}}$ can be found (in the megawatt range) above which the pulse is transformed into a white-light continuum. The resultant beam appears to the eye as a white spot when the beam is projected onto a screen. When the pulse's peak power is just above $P_{\text{th}}^{\text{wl}}$ the white spot has a radius that is comparable with the radius of the pump beam in the linear regime. As the peak power is increased to a few $P_{\text{th}}^{\text{wl}}$ a colorful ring pattern appears, surrounding the central spot. A further increase in peak power causes the diameter of the central white spot to increase and eventually to fill the ring pattern. The resultant appearance is a white solid disk with a blue rim.

Comparison of $P_{\text{th}}^{\text{wl}}$ and $P_{\text{th}}^{\text{sf}}$ in several media shows that $P_{\text{th}}^{\text{wl}} \simeq P_{\text{th}}^{\text{sf}}$ within a $\pm 10\%$ precision. For instance, in water there is continuum generation at $P = 1.0P_{\text{th}}^{\text{sf}}$ but not at $P = 0.9P_{\text{th}}^{\text{sf}}$. This observation confirms that self-focusing triggers continuum generation.[7,9,10]

One can easily find the white-light threshold $P_{\text{th}}^{\text{wl}}$ of a medium by looking at the output beam by eye while varying the input peak power. This is much more convenient than finding the self-focusing threshold $P_{\text{th}}^{\text{sf}}$, which requires imaging the geometrical focus of the beam while varying the power. Therefore, in the following measurements the input peak power will be defined in terms of its ratio to $P_{\text{th}}^{\text{wl}}$. It should then be remembered that $P_{\text{th}}^{\text{wl}}$ and $P_{\text{th}}^{\text{sf}}$ are essentially equivalent. Along the same line, we recall that $P_{\text{th}}^{\text{sf}}$ is equivalent to the theoretical P_{crit} in the approximation of a strictly Kerr nonlinearity and a dispersionless and absorptionless medium.

Examples of continua generated in water, UV-grade fused silica, and NaCl at input peak power $P = 1.1P_{\text{th}}^{\text{wl}}$ are shown in Figs. 3(a), 3(b), and 3(c), which show, respectively, the central, the anti-Stokes, and the Stokes parts of the continuum. These spectra are measured ${\sim}1$ mm after the position where the continuum is fully developed; i.e., f_1 is positioned so the continuum is completely generated ${\sim}1$ mm below the medium's output surface. The spectra of Fig. 3 are acquired with the beam centered on the vertical slit of the spectrograph (50 μm wide) and are an integral of the signal measured along the length of the slit. Note the similarity between the spectra generated in water and in fused silica.

Typical features of the continuum are a modulation near the laser wavelength, smoothness in the wings, and a long anti-Stokes wing. The spectra exhibit a strong Stokes–anti-Stokes asymmetry. The part of the continuum that is perceived as white light represents a small fraction of the pulse energy: In the case of water at $P = 1.1P_{\text{th}}^{\text{wl}}$, only 0.6% of the pulse energy is in the region $\lambda < 650$ nm.

The anti-Stokes wing usually falls off abruptly. We define the anti-Stokes broadening $\Delta\omega_+ = \omega_{\max} - \omega_0$, where $\omega_{\max}$ is the anti-Stokes frequency where the signal
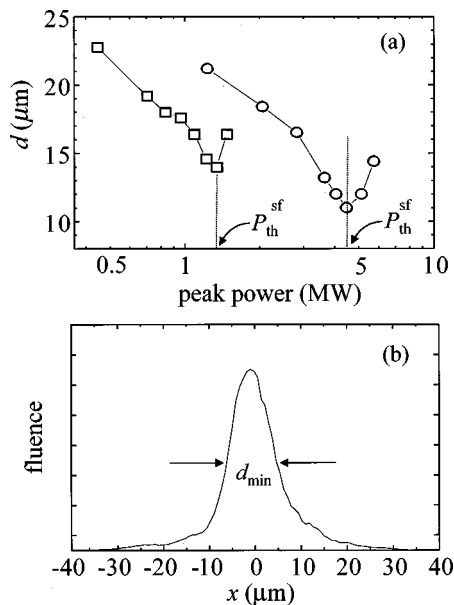

Fig. 2. (a) Beam diameter d (FWHM) at the position of the geometrical focus, as a function of input peak power. Squares, C_2HCl_3 (trichloroethylene); circles, water. (b) Beam profile in water with diameter $d_{\min}$ when $P = 1.1P_{\text{th}}^{\text{sf}}$.
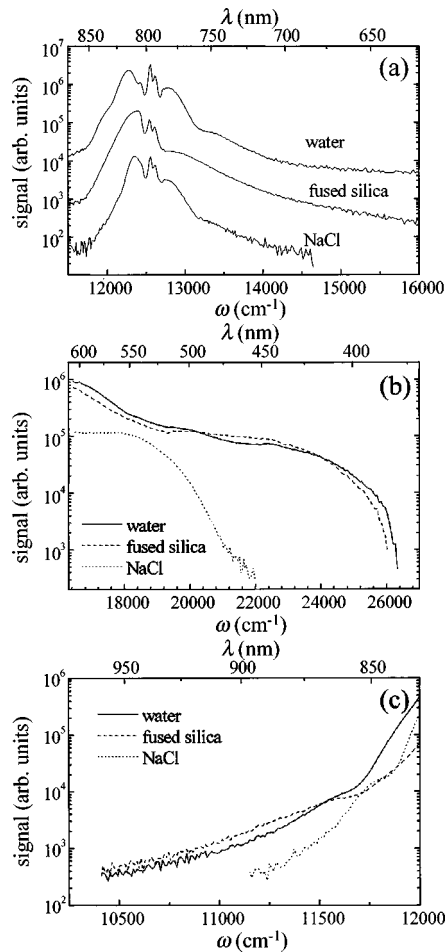
Fig. 3.   Typical white-light continuum spectra generated in water, UV-grade fused silica, and NaCl at $P = 1.1 P_{th}^{wl}$.   (a) Central part.   The curves are shifted vertically for clarity.   (b) Anti-Stokes part.   The intense wavelength components around the laser wavelength are suppressed with a BG18 color filter, which eliminates $\lambda > 630$ nm.   (c) Stokes part.   The intense wavelength components around the laser wavelength are suppressed with a RG850 color filter, which eliminates $\lambda < 850$ nm.   All spectra are corrected for filter, CCD, and grating responses.

drops below the detection threshold and ω_0 is the laser frequency.   Choosing a somewhat higher signal level to define this width would yield essentially the same result because of the abrupt decrease in the signal at the end of the anti-Stokes wing.   The Stokes broadening is defined in a similar manner as $\Delta\omega_- = \omega_{min} - \omega_0$, where ω_{min} is the Stokes frequency where the signal drops below the detection threshold (note that the Stokes wing does not end abruptly as the anti-Stokes wing does).   In this experiment the measured $\Delta\omega_+$ extends over 10 000–20 000 cm^{-1}, depending on the medium, whereas the Stokes broadening $\Delta\omega_-$ is limited to a modest -1000–2000 cm^{-1} in all media.   The spectral extent is not limited by the detector's sensitivity.

The medium that generates the largest anti-Stokes broadening is lithium fluoride (LiF).   The anti-Stokes part of the continuum generated in this medium at $P = 1.1 P_{th}^{wl}$ is shown in Fig. 4.   The spectrum extends well into the ultraviolet.   This spectrum is measured with a different setup that does not include an imaging lens, be-

cause the short wavelengths would be absorbed by imaging lens f_2.   The sample is placed in front of the spectrograph slit, and the beam is focused directly into the sample.

The observed spectra do not exhibit Raman features.   In particular, in water there is no dip at ~630 nm because of inverse Raman scattering involving the 3650-cm^{-1} O—H stretching mode.[5]   We observed such a dip when the peak power strongly exceeded P_{th}.

Figure 5 shows the evolution with propagation distance in water of beam width d, anti-Stokes broadening $\Delta\omega_+$, and pulse energy.   One can see from the top figure that the beam contracts with propagation (left to right in the figure) and reaches a minimum of ~10 μm at $z \sim z_0 - 500\,\mu$m, where z_0 is the geometrical focus.   The beam stays contracted at that diameter up to $z \sim z_0 - 300\,\mu$m and diverges slowly to a diameter of ~11 μm at $z \sim z_0$.   It then diverges more rapidly with further propagation.   Increasing the input peak power leads to a contraction that starts earlier in propagation but still finishes at $z \sim z_0$.

We interpret the region of contracted propagation from $z \sim z_0 - 500\,\mu$m to $z \sim z_0$ as a filament that arises from the moving-focus dynamics: The most powerful slice of
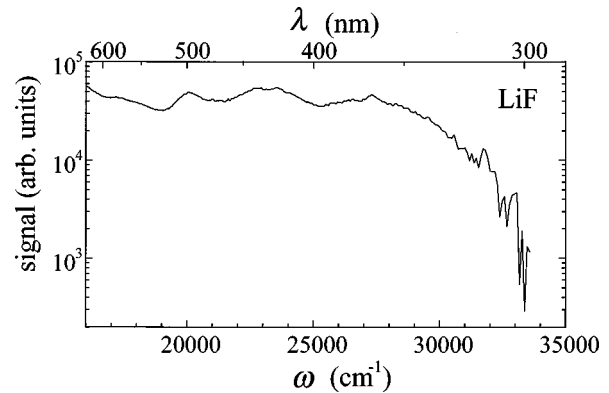

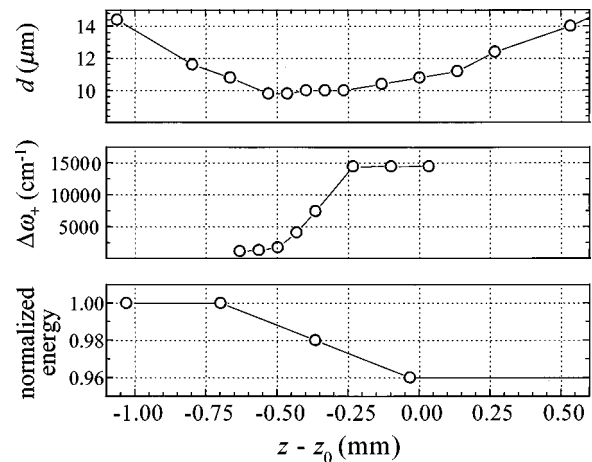Fig. 4.   Anti-Stokes part of the continuum generated in LiF at $P = 1.1 P_{th}^{wl}$.

Fig. 5.   Evolution of FWHM beam width d, anti-Stokes broadening $\Delta\omega_+$, and the pulse energy with propagation distance in water at $P = 1.1 P_{th}^{wl}$. z_0 is the position of the geometrical focus, measured with a precision of $\pm 200\,\mu$m.
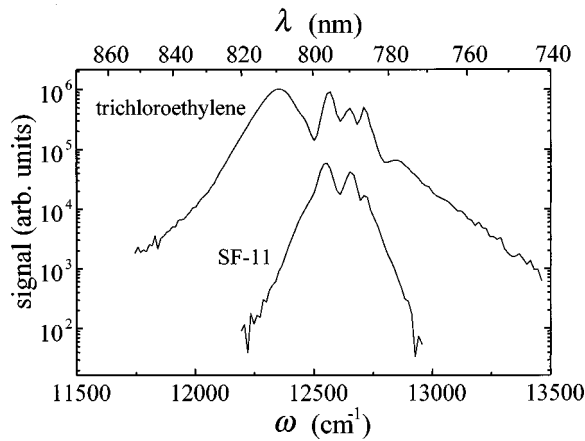
Fig. 6. Spectra generated in trichloroethylene and in SF-11 glass at $P = 1.1 P_{th}^{sf}$. Note the absence of a long anti-Stokes wing.

the pulse self-focuses near $z \sim z_0 - 500\,\mu m$ and the slice with approximately the critical power self-focuses at $z \sim z_0$. The region between these two points is a continuous distribution of self-foci associated with intermediate powers. The observation of a filament that starts earlier along the z axis with higher power is consistent with the moving-focus model. The fact that the end of the filament does not change with power is also consistent with the moving-focus model and with Eq. (3). These concepts have been explored in Refs. 45 and 46 in the context of beam filamentation in air. It should be noted that we observe a second filament alongside the original filament when the peak power is increased to $\sim 5P_{th}$. The length of the original filament is thus limited, because the additional power goes into a new filament rather than into an extension of its length.

One can see from Fig. 5 that the continuum starts to appear when the beam is contracted into a filament. The spectrum broadens rapidly over a distance of $\sim 200\,\mu m$, after which it is a fully developed continuum. The bottom part of Fig. 5 shows that the continuum develops concurrently with an energy loss of a few percent.

C. Media That Cannot Generate a Continuum
The white-light continuum described in Subsection 4.B is not observed in all transparent condensed media. In SF-11 glass, trichloroethylene, benzene, toluene, and CS_2 the pulse is not transformed into a continuum when the peak power exceeds P_{th}^{sf}. The spectrum measured after propagation in one of these media is comparatively much narrower and nearly symmetric (Fig. 6). After propagation in these media the beam remains invisible to the eye when the beam is projected onto a screen; at several P_{th}^{sf} the central part of the beam acquires at best a dim reddish tint. There is no sharp threshold for the appearance of this visible light, and there is no visible light at powers below $P \simeq 10 P_{th}^{sf}$. The appearance of this dim visible light in the forward direction at high power is often accompanied by the appearance of a colorful pattern of conical emission surrounding the beam, similar to that observed in the media that can generate a white-light continuum.

D. Bandgap Dependence of Continuum Generation and Self-Focusing
Investigation of continuum generation and self-focusing in several media revealed a dependence on E_{gap}, the bandgap of the material.[47] The most striking observation is that continuum generation occurs only in media with E_{gap} larger than the threshold $E_{gap}^{th} \simeq 4.7\,eV$. Also surprising is a trend of increasing $\Delta\omega_+$ with increasing E_{gap}. Observation of this trend in several media led us to investigate LiF, the medium with largest E_{gap}. Indeed, LiF yielded the broadest continuum. The dependence of $\Delta\omega_+$ on E_{gap} is shown in Fig. 7(a) and in Table 1, along with various measured self-focal characteristics.

One can see from Table 1 that d_{min} also exhibits a discontinuity at E_{gap}^{th}. Typically, media with $E_{gap} < E_{gap}^{th}$ yield $d_{min} \sim 15\,\mu m$, whereas media with $E_{gap} > E_{gap}^{th}$ yield $d_{min} \sim 10\,\mu m$. This discontinuity translates into a jump in maximum fluence across E_{gap}^{th}. We also point out the trend of increasing maximum fluence with increasing E_{gap} above E_{gap}^{th}, despite the roughly constant d_{min}.

In Table 1, P_{th} designates either P_{th}^{wl}, for media that generate a continuum, or P_{th}^{sf}, for media that do not generate a continuum (we recall that $P_{th}^{wl} \simeq P_{th}^{sf}$). One can see that P_{th} tends to increase with E_{gap}. This implies that the Kerr index n_2 decreases with E_{gap} because the theoretical P_{crit} is inversely proportional to n_2. Therefore $\Delta\omega_+$ increases with decreasing n_2. This observation contradicts the theory of SPM in neutral Kerr media,
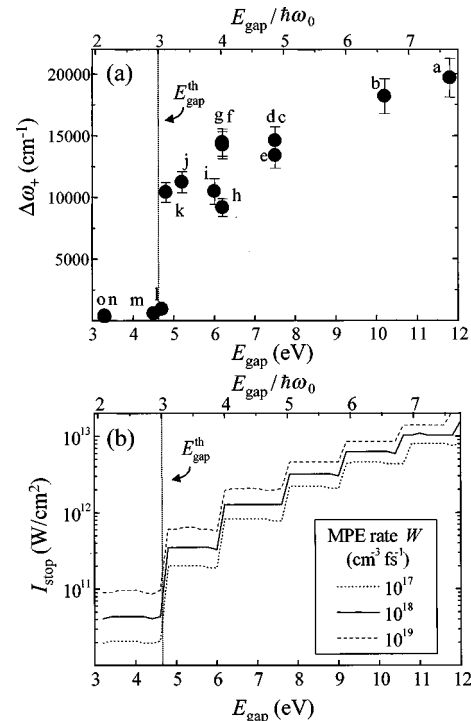

Fig. 7. (a) $\Delta\omega_+$ versus bandgap in various media: a, LiF; b, CaF_2; c, UV-grade fused silica; d, water; e, D_2O; f, 1-propanol; g, methanol; h, NaCl; i, 1,4-dioxane; j, chloroform; k, CCl_4; l, C_2HCl_3; m, benzene; n, CS_2; o, SF-11 glass. (b) Intensity I_{stop} required in Keldysh theory for MPE rate $W = 10^{18}\,cm^{-3}\,fs^{-1}$ as a function of bandgap (solid curve). The curves for $W = 10^{17}$ and $W = 10^{19}\,cm^{-3}\,fs^{-1}$ are displayed for comparison. The top axis shows the bandgap normalized to the laser photon energy.

Table 1. Self-Focal Characteristics Measured in Various Media at $P = 1.1\,P_{th}$[a]

Medium	E_{gap} (eV)	d_{min} (μm)	$\Delta\omega_+$ (cm^{-1})	F_{max} (J/cm^2)	E_{loss} ± 1 (%)	P_{th} (MW)
LiF	11.8	10.8	19 800	1.3	13	8.8
CaF$_2$	10.2	10.4	18 300	1.0	11	7.4
Water	7.5	9.8	14 600	0.62	4	4.4
D$_2$O	7.5	10.6	14 600	0.46	4	3.6
Fused silica	7.5	10.4	13 500	0.57	3	4.3
Propanol	6.2	9.1	14 200	0.57	3	3.3
Methanol	6.2	10.2	14 500	0.54	4	3.9
NaCl	6.2	9.9	9 000	0.29	3	2.0
1,4-Dioxane	6.0	9.3	10 200	0.44	3	2.7
Chloroform	5.2	10.0	11 200	0.29	1	2.2
CCl$_4$	4.8	8.7	10 400	0.44	2	2.5
C$_2$HCl$_3$	4.7	14.6	950	0.08	<1	1.2
Benzene	4.5	14.0	600	0.07	<1	0.90
CS$_2$	3.3	15.6	400	0.01	<1	0.23
SF-11 glass	3.3	15.6	340	0.03	3	0.52

[a] For media with $E_{gap} > E_{gap}^{th} = 4.7$ eV, P_{th} is the measured P_{th}^{wl} (which is $\simeq P_{th}^{sf}$), and for media with $E_{gap} < E_{gap}^{th} = 4.7$ eV, P_{th} is the measured P_{th}^{sf}, d_{min} is the diameter (FWHM) of the beam waist (± 0.5 μm); F_{max} is the maximum fluence; E_{loss} is the percentage of energy loss with respect to the input energy (excluding linear losses).

which predicts an increase of $\Delta\omega_+$ with increasing n_2 [Eqs. (6)–(8)].

5. PROPOSED MECHANISM

A. Limitation of the Self-Focal Diameter by Generation of Free Electrons

To gain insight into the bandgap dependence of the continuum, let us first consider the mechanism that stops the beam's catastrophic collapse in a self-focus. In the case of picosecond pulses, for which self-focal diameters of typically 6–10 μm are observed,[28] the mechanism generally invoked is avalanche ionization of the medium[38,48] (see Subsection 2.B). Questions regarding the mechanism limiting self-focusing for femtosecond pulses were raised initially by Corkum *et al.*[7] Those authors observed that the onset of catastrophic self-focusing leaves the spatial characteristics of the beam practically unchanged after the beam's focus. Furthermore, little energy loss was observed. These observations, which are not expected from avalanche ionization as a limiting mechanism, triggered theoretical work on the connection among self-focusing, GVD, and SPM.[31–34]

The bandgap dependence of the self-focal diameter observed in the present study suggests that free-electron generation by MPE is important in the limitation of self-focusing of 140-fs Ti:sapphire pulses in condensed media. Indeed, the bandgap is an important parameter that governs MPE. We note that the lack of observed Raman activity in our spectra rules out stimulated Raman scattering as the main limiting mechanism.

1. Description of the Mechanism and Estimates

During self-focusing a sharp intensity spike develops in the laser pulse.[20,31,45,46] Assuming that self-focusing is limited by MPE, the index change $n_2 I$ that is due to the Kerr effect should be canceled by Δn_e, which is the index change caused by free electrons [Eq. (4)] that appears at the peak of the intensity spike. In the approximation $\omega_0^2 \gg \nu^2$ this cancellation should occur when

$$n_2 I = \frac{2\pi e^2 N_e}{n_0 m_e \omega_0^2}. \tag{9}$$

To find the intensity I_{stop} and the electron density N_e^{stop} that satisfy this relation, let us examine the MPE rate W in the case of water. Using the Keldysh theory of MPE,[40] we obtain the intensity dependence of W, shown as a solid curve in Fig. 8. We must now determine at which point on this curve Eq. (9) will be satisfied. One can see from the figure that W increases rapidly with intensity; this implies that during self-focusing most of the free electrons appear at the peak of the intensity spike, during the half-cycle (1.3 fs) when the electric field is maximum. The MPE rate required for generation of a free-electron density N_e in one half-cycle is given by

$$W \;[\text{cm}^{-3}/\text{fs}] \sim \frac{N_e \;[\text{cm}^{-3}]}{(1.3 \;\text{fs})}. \tag{10}$$

Combining Eq. (9) and relation (10), we find that the Kerr index is canceled when the MPE rate is

$$W \;[\text{cm}^{-3}/\text{fs}] \sim \frac{n_0 m_e \omega_0^2 n_2 I}{2\pi e^2 (1.3 \;\text{fs})}. \tag{11}$$

This relation is plotted as a dashed curve in Fig. 8. The two curves cross at $I_{stop} \sim 10^{12}$ W/cm^2 and $W_{stop} \sim 10^{18}$ cm^{-3}/fs. Using relation (10), we find that $N_e^{stop} \sim 10^{18}$ cm^{-3}, which is similar to the density required for stopping self-focusing by avalanche ionization.[4,38]

Let us see whether these results are consistent with the experiment. First, we can estimate the free-electron density N_e^{stop} generated in our experiment in water by assuming that MPE accounts for most of the energy loss (a loss of $E_{gap} = 7.5$ eV per generated free electron in water). We approximate the plasma volume to a 200-μm-long cylinder with a diameter that cannot be larger than d_{min}
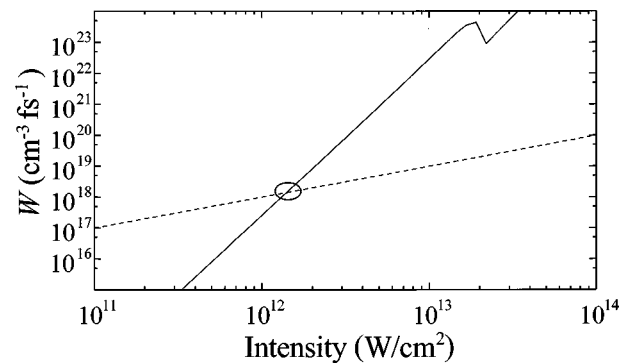

Fig. 8. Intensity and MPE rate at which self-focusing stops in water. Solid curve, the MPE rate versus intensity in water, calculated from the Keldysh theory of MPE. Dashed curve, the MPE rate versus intensity for which the Kerr index and the plasma index cancel in water, from Eq. (9) (assuming that MPE occurs in half of an optical cycle). The point where the two curves cross gives the intensity and MPE rate when self-focusing stops. We use $n_2 = 2 \times 10^{-16}$ cm^2/W, extracted from the measured critical power in water.

= 9.8 μm (see Table 1) and cannot be smaller than ~ 1 μm, the theoretical lower limit set by diffraction.[37] We obtain $1 \times 10^{17} < N_e{}^{\text{stop}} < 1 \times 10^{19}\,\text{cm}^{-3}$, which is consistent with $N_e{}^{\text{stop}} \sim 10^{18}\,\text{cm}^{-3}$ obtained from expressions (9)–(11).

Let us now see whether the experimental self-focal intensity I_{stop} achieved in water is comparable with the calculated value $I_{\text{stop}} \sim 10^{12}\,\text{W/cm}^2$. Beforehand, some attention should be paid to what is actually measured in the experiment. Indeed, the maximum intensity reached in the filament cannot be inferred from the smallest measured diameter $d_{\min}$ along the filament, because $d_{\min}$ is the time-integrated beam diameter. To grasp these concepts fully one has to refer to the moving-focus model of self-focusing (see Subsection 2.A). Under conditions of linear focusing, i.e., when focusing is due solely to an external lens and not to self-focusing, all the slices are focused to the same diameter. The maximum intensity I_{stop} achieved in the focus is then given by $\sim F_{\max}/\tau_0$, where $F_{\max}$ is the maximum fluence and τ_0 is the input pulse duration (FWHM). When self-focusing occurs, however, various longitudinal slices of the pulse contract to different diameters according to the ratio of their own power to P_{crit}. At the position with the smallest measured beam diameter $d_{\min}$, a slice can be self-focused to the limiting diameter d_{limit}, while the rest of the pulse is not focused so tightly. Furthermore, whereas a particular slice with supercritical power might form a self-focus at the position where the measurement is made, other slices with supercritical power might form a self-focus at an earlier or later position along the axis. Those slices would not be contracted to d_{limit} at the position of measurement. For these reasons the measured fluence distribution (time integral of the intensity distribution) has a diameter $d_{\min}$ larger than the actual limiting diameter d_{limit}. As a result, I_{stop} has to be greater than $F_{\max}/\tau_0$.

Using these concepts, we estimate (using $F_{\max}$ = 0.62 J/cm^2; see Table 1) that the self-focal intensity achieved in water at $P = 1.1 P_{\text{th}}^{\text{wl}}$ is greater than $5 \times 10^{12}\,\text{W/cm}^2$. This value is larger than I_{stop} $\sim 10^{12}\,\text{W/cm}^2$, the value obtained from expressions (9)–(11), thus reinforcing the assumption that MPE does occur in the self-focus.

Our estimates of I_{stop} and $N_e{}^{\text{stop}}$ also agree with recent studies of laser-induced breakdown of water,[22,23] which have shown that a 100-fs pulse with a peak intensity of $5 \times 10^{12}\,\text{W/cm}^2$ can generate a free-electron density N_e $\simeq 10^{18}\,\text{cm}^{-3}$. It is therefore reasonable to assume that in our experiment significant MPE occurs in the self-focus and stops self-focusing.

2. Bandgap Dependence
Table 1 shows that $d_{\min}$ is larger in media with E_{gap} $< E_{\text{gap}}^{\text{th}}$ than in media with $E_{\text{gap}} > E_{\text{gap}}^{\text{th}}$. To get some insight into this behavior let us consider the bandgap dependence of MPE in the framework of Keldysh theory.[40] We saw above that MPE should stop self-focusing when the MPE rate reaches $W \sim 10^{18}\,\text{cm}^{-3}\,\text{fs}^{-1}$. The intensity I_{stop} at which this rate is achieved depends on the bandgap. This dependence is shown in Fig. 7(b). The jumps in I_{stop} at $E_{\text{gap}} = m\hbar\omega_0$, where $m = 3, 4, 5...$, indicate the passage from m-photon to $(m + 1)$-photon excitation.

The jump of approximately an order of magnitude at m = 3 is of particular interest inasmuch as it occurs at the measured $E_{\text{gap}}^{\text{th}} \simeq 4.7$ eV. In media with $E_{\text{gap}} < E_{\text{gap}}^{\text{th}}$ self-focusing stops at a low intensity because of MPE, thus explaining the large $d_{\min}$. This observation is consistent with MPE as the mechanism that stops self-focusing.

3. Other Considerations
So far we have neglected avalanche ionization as a mechanism of free-electron generation with 140-fs pulses. At $I = 10^{13}\,\text{W/cm}^2$, the doubling time for the electron density during an avalanche in typical materials is estimated to be longer than ~ 50 fs, based on dielectric breakdown measurements in NaCl.[38] This implies ~ 3 doubling generations in a 140-fs pulse. However, approximately 30 doubling generations are needed to build up a 10^{17}–10^{18}-cm^{-3} electron density by avalanche ionization,[4] thus requiring an ~ 1.5-ps pulse duration. The pulse in this experiment is thus too short for avalanche ionization to account entirely for the calculated density. The calculations of Feng et al.[23] show that, in water, avalanche ionization can be completely neglected for pulse durations of ~ 40 fs or less. According to their calculations, although MPE dominates in the femtosecond regime there is still a contribution from avalanche ionization. However, because avalanche ionization takes time to build up it should be more important in the back of the pulse than in the front, and it should not be involved in the limitation of the self-focus at the front of the pulse, which occurs on a short time scale. Furthermore, self-focusing should be weaker at the back of the pulse because of defocusing by electrons generated at the front of the pulse. Therefore our neglect of avalanche processes should not have a significant effect on our analysis of the limitation of the self-focal diameter.

Besides inducing defocusing, MPE also causes an energy loss. This implies a reduction of power that can stop catastrophic self-focusing. During self-focusing only the supercritical section of the pulse, i.e., the section where the power exceeds P_{crit}, suffers the onset of catastrophic self-focusing and the energy loss that are due to MPE. Most of the pulse suffers only a radial contraction followed by defocusing owing to diffraction. This explains the somewhat small measured energy losses. The energy loss in the supercritical section of the pulse translates into a localized reduction of power. Assuming a Gaussian input pulse with peak power $P = 1.1 P_{\text{crit}}$, approximately one third of the pulse energy is localized in the section of the pulse with power that exceeds P_{crit}. A typical energy loss of 5% then translates into a reduction of power of $\sim 25\%$ in the supercritical section of the pulse. The section thus becomes subcritical, and catastrophic self-focusing is stopped. This MPE-linked mechanism would combine with electron defocusing to stop self-focusing.

B. White-Light Continuum from Self-Phase Modulation Enhanced by Free-Electron Generation
The mechanism usually invoked to explain the ultrafast continuum is SPM in a neutral Kerr medium.[8] However, the results presented here are not consistent with that model. For instance, Eq. (8) is unable to account for the

large measured spectral asymmetry. In water we observe $\Delta\omega_- \simeq -0.15\omega_0$. This value corresponds to $Q \simeq 0.3$ in Eq. (8), which in turn implies that $\Delta\omega_+ \simeq -0.16\omega_0$, i.e., a nearly symmetric spectrum where $\Delta\omega_+ \simeq 1.07\Delta\omega_-$. Inclusion of self-steepening does not significantly increase this asymmetry when $Q \simeq 0.3$.[8] The theoretical asymmetry is thus clearly insufficient compared with the measured asymmetry, $\Delta\omega_+ \simeq 7\Delta\omega_-$. In addition, we observe an increase of $\Delta\omega_+$ with decreasing Kerr nonlinearity, which is contrary to the prediction of usual SPM theory.

Four-wave mixing can also cause a large spectral broadening.[3,12,14] However, in the regime that we investigated the white-light beam has a narrow divergence of less than 1.3 deg (see Section 6 below). This narrow divergence is not consistent with the phase-matching requirements of four-wave mixing. Furthermore, a strong decrease in spectral density should be observed near 400 nm, i.e., at twice the laser frequency, because shorter wavelengths would require higher-order processes. The limitations of four-wave-mixing in explaining continuum generation are discussed in Ref. 5. It is, however, likely that four-wave mixing plays a role in continuum generation at regimes well above threshold.[12,14] Note that four-wave mixing has been proposed to explain the conical emission that surrounds the on-axis continuum beam, because it predicts an angular spread of the generated frequencies owing to phase-matching considerations.[49] However, the conical emission could also arise from spatial SPM in a plasma during continuum generation.[46]

The observed spectra do not exhibit Raman features. The absence of observed Raman activity can be attributed to the fact that in our experiment only a small portion of the pulse undergoes critical self-focusing because the peak power exceeds P_{th} by only 10%. This translates into an intensity spike that is too short for Raman modes to be activated. A strong Raman contribution to continuum generation should also translate into a large Stokes broadening, which is not observed.

In this light, it is clear that another mechanism should be invoked to explain continuum generation. We consider the enhancement of SPM by generation of free electrons through MPE.

1. Description of the Mechanism

The fact that continuum generation is triggered by the onset of catastrophic self-focusing suggests that free electrons may be involved in continuum generation. Such a mechanism was first proposed by Bloembergen to explain the picosecond continuum, in the form of SPM enhancement by avalanche ionization.[4,5] The situation is somewhat different with femtosecond pulses, for which the main mechanism of free-electron generation in a condensed medium is MPE.[22,23,40]

We can explain the continuum observed in this experiment by reviving Bloembergen's model of ionization-enhanced SPM[4,5] in the context of femtosecond pulses and MPE. We see from Eq. (7) that in conventional SPM theory the anti-Stokes broadening is proportional to the maximum rate of decrease of the nonlinear phase. To include self-focusing in this picture we should first consider the nonlinear phase in the moving-focus model.[4] During self-focusing a sharp intensity spike develops first at the center of the pulse. The intensity of this spike reaches a maximum I_{stop}, at which point the spike generates free electrons and is defocused. Slices with slightly less power form their own self-foci further along the propagation axis. In other words, the spike splits into two: One spike moves toward the front of the pulse, and the other moves toward the back of the pulse. However, the back of the pulse propagates through the free electrons generated by slices ahead such that self-focusing is weaker at the back of the pulse.[23,45,46] The spike at the front of the pulse propagates in a neutral medium and causes a large nonlinear index change. As the spike moves toward the front of the pulse, a large nonlinear phase ϕ_{NL} accumulates in the front of the pulse. Because the appearance of free electrons occurs in a very short time (which in Subsection 5.A we estimate to be half of an optical cycle), the drop in index following the peak of the spike also occurs in a short time. The drop in nonlinear phase near the middle of the pulse is therefore quite sharp and translates into a large anti-Stokes broadening. The increase in nonlinear phase at the front of the pulse is much more gradual and results in a smaller Stokes broadening.

2. Numerical Simulations

The mechanism described was simulated in a one-dimensional calculation of pulse propagation in water. For the calculations the pulse is segmented into discrete temporal slices at intervals $\delta t = 0.25$ fs. The distance along the propagation axis from the self-focus of the most powerful slice to the self-focus of a slice with critical power is divided into 1000 segments of length δz (at $P = 1.1P_{\mathrm{crit}}$, $\delta z \simeq 0.5\,\mu\mathrm{m}$). We assume that only the slices in the leading half of the pulse self-focus, because the trailing half propagates in the track of free electrons left behind by the front of the pulse.

We calculate the position of the self-focus associated with each temporal slice τ_i with power exceeding P_{crit} from Eqs. (2) and (3), using the focusing geometry of the experiment. For each of these slices a nonlinear index change $\Delta n_i(t)$ is assigned to the point in the medium where the self-focus is formed. The nonlinear phase ϕ_{NL} of the slices in the vicinity of slice τ_i is then incremented by an amount determined by $\Delta n_i(t)$: The nonlinear phase ϕ_{NL}^{i-1} of slice τ_{i-1} is incremented by $\Delta\phi_{\mathrm{NL}}^{i-1} = (2\pi/\lambda_0)\Delta n_i(\tau_{i-1})\delta z$, the nonlinear phase ϕ_{NL}^{i} of slice τ_i is incremented by $\Delta\phi_{\mathrm{NL}}^{i} = (2\pi/\lambda_0)\Delta n_i(\tau_i)\delta z$, and so on. With this procedure the ϕ_{NL} accumulated throughout the pulse is obtained. The resultant spectrum is then computed by a fast Fourier transform.

The total index change $\Delta n_i(t)$ associated with the self-focus of slice τ_i is a combination of the Kerr and the free-electron index changes. $\Delta n_i(t)$ is assigned the following simple temporal distribution[21] [Fig. 9(a)]: $\Delta n_i(t)$ increases linearly during $t_{\mathrm{rise}} = 100$ fs, reaches a maximum n_2I_{stop}, and then drops to zero over $t_{\mathrm{fall}} = 1.3$ fs. The slow increase in $\Delta n_i(t)$ is due to the Kerr index associated with the slices in front of slice τ_i. The rapid drop in Δn_i is due to the cancellation of the Kerr index by the free electrons generated during half of an optical cycle. Note that Δn_i is taken to be positive at all times. This approximation should not affect the qualitative behavior of the re-

sultant spectrum, because spectral broadening depends on the rate of change of Δn_i, not on its magnitude. To account for the defocusing that is due to free electrons, only the leading half of the pulse is allowed to self-focus.

A simulation of the propagation in water was performed with input peak power $1.1 P_{crit}$, $n_2 = 2 \times 10^{-16}\,cm^2/W$ (estimated from the measurements in water), and a maximum intensity $I_{stop} = 1 \times 10^{13}\,W/cm^2$. The propagation leads to a 506-μm long filament that ends at the geometrical focus of the focusing lens, in agreement with the measured filament shown in Fig. 5. The simulation yields the dashed-curve spectrum in Fig. 9(b). The general shape of the calculated spectrum is similar to that of the measured spectrum (solid curve), showing a long but weak anti-Stokes wing. For comparison the corresponding simple SPM spectrum is shown as a dotted curve. We calculated the simple SPM spectrum by assuming the Gaussian intensity distribution with maximum intensity $1 \times 10^{13}\,W/cm^2$ sustained over 500 μm. Note the similarity of the Stokes side of the simple SPM spectrum to the measured spectrum; the main discrepancy lies on the anti-Stokes sides of the spectra.
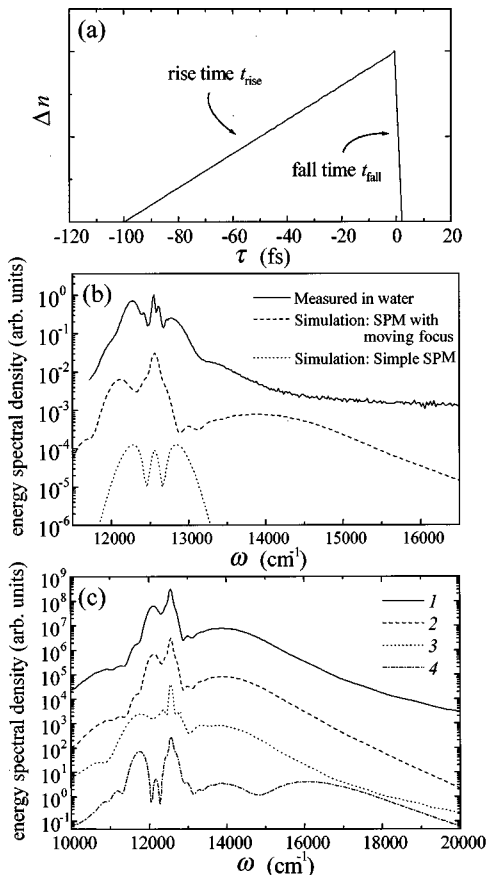

Fig. 9.   (a) Time dependence of the total change in refractive index at a self-focus in the simulation.   (b) Continuum spectra generated water at $P = 1.1 P_{crit}$ in the experiment, in a one-dimensional simulation including the moving-focus dynamics under MPE conditions, and in simple SPM.   (c) Simulated spectra associated with the following respective values of t_{rise}, t_{fall} and I_{stop}:   *1*, 100 fs, 1.3 fs, $10^{13}\,W/cm^2$; *2*, 100 fs, 5 fs, $10^{13}\,W/cm^2$; *3*, 50 fs, 5 fs, $10^{13}\,W/cm^2$; *4*, 100 fs, 5 fs, $2 \times 10^{13}\,W/cm^2$.   The spectra are vertically shifted for clarity.

The numerical model does not depend strongly on the assigned $\Delta n(t)$, as we can see from Fig. 9(c), which shows the spectra that correspond to various values of t_{rise} and t_{fall}. The strongest dependence is on the intensity I_{stop} achieved in the self-focus. The effect of doubling I_{stop} from 1×10^{13} to $2 \times 10^{13}\,W/cm^2$ is shown by spectra *1* and *4* of Fig. 9(c). The anti-Stokes wing is more important at the higher intensity.

The simplified model presented here can therefore explain the principal features of the observed continua. The main discrepancy between the simulated and the measured spectra lies in the anti-Stokes wing of the spectrum, which falls off faster in the simulation than in the experiment. A better description would require more-rigorous calculations, which are beyond the scope of this study.

3. Bandgap Dependence

Now that we have established MPE-enhanced SPM as a plausible mechanism for continuum generation, let us see how it can explain the observed dependence of $\Delta \omega_+$ on the bandgap of the medium. To this end, we again turn to the Keldysh theory of MPE in condensed media, as was done in Subsection 5.A to explain the bandgap dependence of the measured self-focal diameter.

Let us first look at the dependence of $\Delta \omega_+$ on E_{gap} and compare it with the dependence on E_{gap} of the intensity I_{stop} required for stopping self-focusing. Comparing Figs. 7(a) and (b), we can see that I_{stop} is larger in media with $E_{gap} > E_{gap}^{th}$ than in media with $E_{gap} < E_{gap}^{th}$. There is indeed a jump in I_{stop} at E_{gap}^{th}, which is due to the passage from three- to four-photon MPE. Similarly, we see from Fig. 7(a) that a continuum is generated only in media with $E_{gap} > E_{gap}^{th}$. We can deduce that the intensity achieved in the latter is sufficient to accumulate enough nonlinear phase for continuum generation. In media with $E_{gap} < E_{gap}^{th}$ self-focusing is stopped by free-electron defocusing before an intensity sufficient for continuum generation is achieved.

The increase of I_{stop} with E_{gap} is also consistent with the observed trend of increasing $\Delta \omega_+$ with increasing E_{gap}. A higher I_{stop} implies the accumulation of a larger nonlinear phase and thus larger broadening. The numerical simulations of Subsection 5.B.2 showed that an increase in I_{stop} indeed leads to an increase in anti-Stokes broadening. The fact that no clear discontinuities are observed in continuum behavior at $E_{gap} = 6.2, 7.8,...eV$ could be due to the modification of the band structure in the presence of an intense field.[50]

4. Other Considerations

The effect of GVD on pulse propagation has not been included in the proposed mechanism. A possible consequence of GVD could be the splitting of the pulse during self-focusing[15,33,35,36] before the occurrence of MPE. The effect of this splitting is similar to the effect discussed above of the splitting of the intensity spike in the moving-focus model. The MPE that causes strong anti-Stokes SPM occurs in the intensity peak at the front the pulse and causes the peak at the back of the pulse to defocus.

We remark that continua generated in gases[7,10] generally exhibit a weak dependence of $\Delta\omega_+$ on the medium (i.e., gas species) and a nearly symmetric spectrum, unlike the continua of this experiment. Continua from gases are also narrower ($\Delta\omega_+ \simeq 0.5\omega_0$) than those from condensed media ($\Delta\omega_+ \simeq 0.8\omega_0 - 1.6\omega_0$). The contribution of free electrons to continuum generation could therefore be more important in condensed media than in gases.

6. ANOMALOUS DIVERGENCE OF THE CONTINUUM BEAM

The femtosecond continuum generated in condensed media at powers just above P_{th}^{wl} has a divergence that is comparable with the divergence of the pump beam in the linear regime. This observation is surprising, considering that self-focusing should play an important role in continuum generation. Indeed, during self-focusing the beam collapses to a small diameter, which should imply a large continuum divergence. This observation suggests the absence of a self-focus; it is in part the observation of a small continuum divergence by Corkum $et\ al.$[7] that triggered theoretical work on the interplay of self-focusing, self-phase modulation, and GVD.[15,31-34] In this section we show that the anomalous low divergence of the continuum beam is actually due to a self-guiding mechanism that channels the white-light beam after its generation in a self-focus.

Measurements of the divergence of the white-light continuum generated in fused silica at $P = 1.1 P_{th}^{wl}$ are performed with the setup of Fig. 10(a). We perform measurements at various wavelengths by sending the beam through an interference filter (10-nm bandwidth) onto the slit of the spectrograph. The FWHM diameter of the recorded beam is measured along the slit axis. The divergence angle is defined as the ratio of the beam diameter
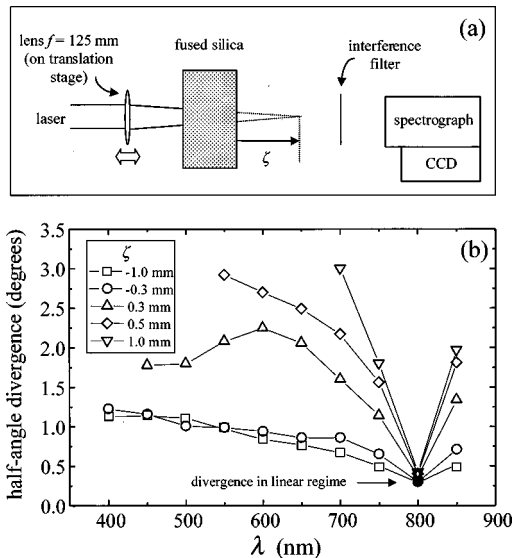

on the slit to the distance from the sample's output surface to the spectrograph slit. We can change the distance ζ from the output surface of the sample to the geometrical focus of the lens by moving the focusing lens, which results in the output surface's coinciding with a different stage of propagation. We calibrate ζ by using the fact that at $P = 1.1 P_{th}^{wl}$ the continuum appears $\sim$500 μm before the geometrical focus along the propagation axis (see Section 4). This means that when focusing lens f_1 is positioned such that the continuum is generated just beneath the sample's output surface, the geometrical focus is $\sim$500 μm above the output surface, and we set $\zeta = 0.5$ mm.

The beam divergence of the continuum generated in fused silica is shown in Fig. 10(b) as a function of wavelength. One can see that the overall divergence of the continuum is lowest when the geometrical focus is inside the sample, at $\zeta = -1.0$ mm and $\zeta = -0.3$ mm. In these cases the continuum is generated well inside the medium. The overall divergence of the continuum is larger when $\zeta = 0.3$ mm and the continuum is generated closer to the surface (at this point the geometrical focus is outside the sample) and is even larger when it is generated just beneath the output surface at $\zeta = 0.5$ mm. At $\zeta = 1.0$ mm there is no white-light generation, although there is spectral broadening, but the divergence at wavelengths $\lambda = 700, 750, 850$ nm is larger than at the previous values of ζ.

It is clear from these observations that the continuum beam has a lower divergence when it is allowed to propagate in the medium for some distance after its generation. For instance, going from $\zeta = -0.3$ mm to $\zeta = 0.3$ mm reduces the overall divergence by a factor of $\sim$2. There is thus a self-guiding effect taking place after the self-focus. This effect can be described in the following manner: Once white light is generated near the axis it starts to diverge because of diffraction and of the free electrons located on the axis. However, the high-intensity beam that generated the white light is also expanding but at a reduced rate (because of the Kerr lens that it induces). While the high-intensity beam is expanding it guides the white light beam and reduces its far-field divergence.

The observation of a low continuum divergence is therefore not inconsistent with self-focusing as a triggering mechanism, as was suspected by Corkum $et\ al.$[7] In fact, the large divergence observed when the continuum is generated close to the surface is evidence that strong self-focusing has occurred. For instance, at $\zeta = 0.5$ mm the divergence at $\lambda = 600$ nm is $\sim$3 deg, which is approximately ten times larger than the divergence of the input beam in the linear regime. The source size at $\lambda = 600$ nm should therefore be less than $\sim$3 μm (i.e., more than ten times smaller than the input beam's focal diameter in the linear regime) and not much larger than the lower limit of $\sim$1 μm set by diffraction.[37]

Fig. 10. (a) Setup used for divergence measurements. ζ is the distance between the sample's output surface and the geometrical focus. (b) Divergence of the continuum beam generated in UV-grade fused silica. The divergence is shown as a function of wavelength for various values of distance ζ from the output surface of the sample to the geometrical focus.

7. SUMMARY

In this paper we have investigated white-light continuum generation and self-focusing in transparent condensed media, using 140-fs Ti:sapphire laser pulses. An inti-

mate connection was established between the two phenomena, as their threshold powers coincide.

The investigation revealed four features of the continuum: (i) a bandgap threshold for continuum generation, (ii) an increase of continuum width with increasing bandgap (i.e., decreasing Kerr nonlinearity), (iii) a very strong Stokes–anti-Stokes asymmetry of the continuum (anti-Stokes wing much larger than Stokes wing), and (iv) an energy loss of a few percent during continuum generation. Furthermore, the self-focal diameter was found to be smaller above the bandgap threshold than below.

SPM theory, which is generally thought to explain the continuum, is not consistent with these features. We have proposed a mechanism that involves free-electron generation in the self-focus by multiphoton excitation; the free electrons would be responsible for enhancing anti-Stokes broadening and for limiting the beam collapse that is due to self-focusing. The proposed mechanism is consistent with the observations enumerated in the previous paragraph. A one-dimensional numerical simulation of continuum generation was presented that supports the proposed mechanism.

Finally, the low beam divergence of the continuum was explained in terms of a Kerr-lens effect in the beam periphery. It was shown that this low divergence does not imply the absence of strong self-focusing in continuum generation.

ACKNOWLEDGMENTS

*Present address, Division of Engineering and Applied Sciences, Harvard University, 9 Oxford Street, Cambridge, Massachusetts 02138.

REFERENCES AND NOTES

1. R. R. Alfano and S. L. Shapiro, Phys. Rev. Lett. **24**, 584 (1970).
2. R. R. Alfano, ed., *The Supercontinuum Laser Source* (Springer-Verlag, New York, 1989).
3. A. Penzkofer, A. Laubereau, and W. Kaiser, Phys. Rev. Lett. **31**, 863 (1973); A. Penzkofer, Opt. Commun. **11**, 275 (1974); A. Penzkofer, A. Seilmeier, and W. Kaiser, Opt. Commun. **14**, 363 (1975).
4. N. Bloembergen, Opt. Commun. **8**, 285 (1973).
5. W. L. Smith, P. Liu, and N. Bloembergen, Phys. Rev. A **15**, 2396 (1977).
6. R. L. Fork, C. V. Shank, C. Hirlimann, R. Yen, and W. J. Tomlinson, Opt. Lett. **8**, 1 (1983).
7. P. B. Corkum, C. Rolland, and T. Srinivasan-Rao, Phys. Rev. Lett. **57**, 2268 (1986); P. B. Corkum and C. Rolland, IEEE J. Quantum Electron. **25**, 2634 (1989); in Ref. 2, pp. 318–336.
8. G. Y. Yang and Y. R. Shen, Opt. Lett. **9**, 510 (1984).
9. V. François, F. A. Ilkov, and S. L. Chin, J. Phys. B **25**, 2709 (1992); Opt. Commun. **99**, 241 (1993).
10. F. A. Ilkov, L. Sh. Ilkova, and S. L. Chin, Opt. Lett. **18**, 681 (1993).
11. G. S. He, G. C. Xu, Y. Cui, and P. N. Prasad, Appl. Opt. **32**, 4507 (1993).
12. A. Penzkofer, A. Beidoun, and H.-J. Lehmeier, Opt. Quantum Electron. **25**, 317 (1993).
13. A. Brodeur, F. A. Ilkov, and S. L. Chin, Opt. Commun. **129**, 193 (1996).
14. M. Wittman and A. Penzkofer, Opt. Commun. **126**, 308 (1996).
15. J. Ranka, R. W. Schirmer, and A. Gaeta, Phys. Rev. Lett. **77**, 3783 (1996).
16. K. R. Wilson and V. V. Yakovlev, J. Opt. Soc. Am. B **14**, 444 (1997).
17. E. N. Glezer, Y. Siegal, L. Huang, and E. Mazur, Phys. Rev. B **51**, 6959 (1995).
18. Q. Z. Wang, P. P. Ho, and R. R. Alfano, in Ref. 2, pp. 39–90.
19. Q. X. Li, T. Jimbo, P. P. Ho, and R. R. Alfano, Appl. Opt. **25**, 1869 (1986).
20. J. H. Marburger, Prog. Quantum Electron. **4**, 35 (1975).
21. Y. R. Shen, Prog. Quantum Electron. **4**, 1 (1975).
22. P. K. Kennedy, IEEE J. Quantum Electron. **31**, 2241 (1995); P. K. Kennedy, S. A. Boppart, D. X. Hammer, B. A. Rockwell, G. D. Noojin, and W. P. Roach, IEEE J. Quantum Electron. **31**, 2250 (1995).
23. Q. Feng, J. V. Moloney, A. C. Newell, E. M. Wright, K. Cook, P. K. Kennedy, D. X. Hammer, B. A. Rockwell, and C. R. Thompson, IEEE J. Quantum Electron. **33**, 127 (1997).
24. E. Garmire, R. Y. Chiao, and C. H. Townes, Phys. Rev. Lett. **16**, 347 (1966).
25. M. M. T. Loy and Y. R. Shen, Phys. Rev. Lett. **22**, 994 (1969); **25**, 1333 (1970); Appl. Phys. Lett. **19**, 285 (1971).
26. A. Brodeur and S. L. Chin, in *Quantum Electronics and Laser Science Conference (QELS)* Vol. 12 of 1997 OSA Technical Digest Series (Optical Society of America, Washington, D.C., 1997), p. 71.
27. A. Brodeur and S. L. Chin, Phys. Rev. Lett. **80**, 4406 (1998).
28. R. G. Brewer and C. H. Lee, Phys. Rev. Lett. **21**, 267 (1968).
29. V. I. Talanov, JETP Lett. **11**, 199 (1970).
30. S. A. Akhmanov, V. A. Vysloukh, and A. S. Chirkin, *Optics of Femtosecond Laser Pulses* (American Institute of Physics, New York, 1992).
31. D. Strickland and P. B. Corkum, Proc. SPIE **1413**, 54 (1991); J. Opt. Soc. Am. B **11**, 492 (1994).
32. P. Chernev and V. Petrov, Opt. Lett. **17**, 172 (1992).
33. J. Rothenberg, Opt. Lett. **17**, 583 (1992).
34. G. G. Luther, J. V. Moloney, A. C. Newell, and E. M. Wright, Opt. Lett. **19**, 862 (1994).
35. S. A. Diddams, H. K. Eaton, A. A. Zozulya, and T. S. Clement, Opt. Lett. **23**, 379 (1998).
36. J. K. Ranka and A. L. Gaeta, Opt. Lett. **23**, 534 (1998).
37. M. D. Feit and J. A. Fleck, J. Opt. Soc. Am. B **5**, 633 (1988).
38. E. Yablonovitch and N. Bloembergen, Phys. Rev. Lett. **29**, 907 (1972).
39. Yu. P. Raizer, Sov. Phys. Usp. **8**, 650 (1966).
40. L. V. Keldysh, Sov. Phys. JETP **20**, 1307 (1965).
41. N. W. Ashcroft and N. D. Mermin, *Solid State Physics* (Saunders, Philadelphia, Pa., 1976).
42. M. Maier, W. Kaiser, and J. A. Giordmaine, Phys. Rev. **177**, 580 (1969).
43. F. Shimizu, Phys. Rev. Lett. **19**, 1097 (1967).
44. R. W. Boyd, *Nonlinear Optics* (Academic, Boston, Mass., 1992).
45. A. Brodeur, O. G. Kosareva, C.-Y. Chien, F. A. Ilkov, V. P. Kandidov, and S. L. Chin, Opt. Lett. **22**, 304 (1997).
46. O. G. Kosareva, V. P. Kandidov, A. Brodeur, C.-Y. Chien, and S. L. Chin, Opt. Lett. **22**, 1332 (1997).
47. The band gap is readily obtained from the absorption spectrum of the medium, which generally shows a sharp absorption edge in the UV that corresponds to the edge of the conduction band. We apply the same definition of E_{gap} to crystals, liquids, and amorphous solids, although the band structures are not so clearly defined in liquids and amorphous solids as in crystals. The relevant physical quantity is the energy that corresponds to the absorption edge. The absorption spectra are obtained from measurements with a

spectrophotometer and from the Photoelectric Spectrom etry Group (London) and the Institut fur Spektrochemie und Angewandte Spektroskopie (Dortmund), *UV Atlas of Organic Compounds* (Butterworth, London, 1966), Vol. 1, Sec. M; O. Madelung, ed., *Landolt–Bornstein Numerical Data and Functional Relationships in Science and Technology*, New Series (Springer-Verlag, Berlin, 1962), Vol. I/4, p. 872; H. H. Jaffé and M. Orchin, *Theory and Application of Ultraviolet Spectroscopy* (Wiley, New York, 1962); J. A. R.

Samson, *Techniques of Ultraviolet Spectroscopy* (Wiley, New York, 1967); L. R. Koller, *Ultraviolet Radiation* (Wiley, New York, 1965).
48. D. H. Auston, in *Ultrashort Light Pulses*, S. L. Shapiro, ed. (Springer-Verlag, New York, 1977), pp. 123–201.
49. Q. Xing, K. M. Yoo, and R. R. Alfano, Appl. Opt. **32**, 2087 (1993).
50. F. H. M. Faisal, J. Phys. B **6**, L89 (1973).